SCIENCE CHINA
Physics, Mechanics & Astronomy

• **Research Paper** •

September 2011 Vol.54 No.9: 1666–1679
doi: 10.1007/s11433-011-4403-0

A magnetically impermeable and electrically permeable interface crack with a contact zone in a magnetoelectroelastic bimaterial under concentrated magnetoelectromechanical loads on the crack faces

FENG WenJie[1*], MA Peng[1], PAN ErNian[2] & LIU JinXi[1]

[1] *Department of Engineering Mechanics, Shijiazhuang Tiedao University, Shijiazhuang 050043, China;*
[2] *Department of Civil Engineering, The University of Akron, Akron, OH 44329, USA*

Received February 10, 2011; accepted May 3, 2011; published online July 18, 2011

An interface crack with a frictionless contact zone at the right crack-tip between two dissimilar magnetoelectroelastic materials under the action of concentrated magnetoelectromechanical loads on the crack faces is considered. The open part of the crack is assumed to be magnetically impermeable and electrically permeable. The Dirichlet–Riemann boundary value problem is formulated and solved analytically. Stress, magnetic induction and electrical displacement intensity factors as well as energy release rate are thus found in analytical forms. Analytical expressions for the contact zone length have been derived. Some numerical results are presented and compared with those based on the other crack surface conditions. It is shown clearly that the location and magnitude of the applied loads could significantly affect the contact zone length, the stress intensity factor and the energy release rate.

interface crack, magnetoelectroelastic bimaterial, concentrated loads, contact zone length, fracture behaviors

PACS: 44.05.+e, 46.25.Hf, 46.50.+a, 77.65.-j

1 Introduction

Magnetoelectroelastic materials have been widely used in electronics industry. The technical applications include waveguides, sensors, phase invertors, transducers, etc. [1]. In the design of magnetoelectroelastic structures, it is important to take into account the defects/imperfections, such as cracks, which are often pre-existing or are generated by external loads during the service life. Therefore, in recent years, research on fracture mechanics of magnetoelectroelastic materials has drawn much attention [2–19].

For two-dimensional (2-D) plane crack problems, Liu et al. [20] derived the general Green's function for an infinite magnetoelectroelastic plane containing an elliptic cavity where they reduced it to solve a permeable crack in the system. Gao et al. [21,22] analyzed single and collinear cracks in an infinite magnetoelectroelastic material and obtained the extended stress intensity factors. Song and Sih [23] and Sih et al. [24] investigated the influence of both magnetic and electric fields on the crack growth, in particular, on the crack initiation angle under various crack surface conditions for Mode-I, Mode-II, and mixed mode crack models. Tian and Gabbert [25,26] studied the interaction of multiple arbitrarily oriented and distributed cracks and of macrocrack-microcrack in homogeneous magnetoelectroelastic materials. Wang and Mai [27] discussed the effects of four kinds of ideal magnetoelectrical crack-face conditions on fracture properties of magnetoelectroelastic materials. Zhong and Li [28] obtained the T-stress for a Griffith crack in an infinite

*Corresponding author (email: wjfeng9999@yahoo.com)

magnetoelectroelastic medium based on magnetic and electric boundary conditions which are nonlinearly dependent on the crack opening displacement. Zhou et al. [29,30] investigated the static fracture behaviors of cracks in piezoelectric/piezomagnetic materials by the Schmidt method. Chen [31] considered the energy release rate and path-independent integral in the dynamic fracture of magneto-electro-thermo-elastic solids. Zhong et al. [32] investigated the transient response of a magnetoelectroelastic solid with two collinear dielectric cracks under impacts.

However, all the above-mentioned work is related to cracks in a homogenous magnetoelectroelastic medium. Due to the oscillating singularity on the crack tip [33,34], the study of interface crack between dissimilar magnetoelectroelastic materials is very limited. Gao et al. [35] and Gao and Noda [36] derived the exact solution for a permeable interface crack between two dissimilar magnetoelectroelastic solids under general loads. Li and Kardomateas [37] investigated the interface crack problem of dissimilar piezoelectromagneto-elastic anisotropic bimaterials under in- plane deformation taking the electric-magnetic field inside the interface crack into account. Feng et al. [38,39] considered both the static and dynamic fracture problems of interface cracks between two dissimilar magnetoelectroelastic layers. Li et al. [40] analyzed the magnetoelectroelastic field induced by a crack terminating at the interface of a bi-magnetoelectrical material. It is worth mentioning that recently Zhao et al. [41] further analyzed the planar interface crack behavior in three-dimensional (3-D) transversely isotropic magnetoelectroelastic bimaterials, and that Zhu et al. [42] investigated the mixed-mode stress intensity factors of 3-D interface crack in fully coupled magneto-electro-thermo-elastic multiphase composites, where the extended hypersingular intergal-differential equation method was used.

On the other hand, as is well known, by introducing the contact zone model, the oscillating singularity can be effectively eliminated [43–46]. Qin and Mai [47], Herrmann and Loboda [48] and Herrmann et al. [49] developed the contact zone model for solving the interface crack problems of piezoelectric bimaterials. However, to the best of our knowledge, up to now, there is only one paper on the contact zone model for an interface crack between two dissimilar magnetoelectroelastic materials [50], where two kinds of magnetoelectrical boundary conditions, i.e., magnetoelectrically permeable, magnetically impermeable and electrically permeable, were considered. For the crack problems under concentrated loads, only the magnetoelectrically permeable interface crack model was analytically investigated [50].

In this paper, therefore, we analyze the interface crack problem under the action of concentrated magnetoelectromechanical loads by introducing the contact zone model, where the magnetically impermeable and electrically permeable crack surface condition is assumed. After some complicated mathematics manipulations, the contact zone length, field intensity factors (including stress, magnetic induction and electrical displacement intensity factors) and energy release rate are derived analytically, and numerical results are further presented to show the effect of the location and magnitude of the loading on these important physical quantities. The solutions and numerical results presented below are applicable to the magnetically impermeable and electrically permeable case unless otherwise indicated.

2 Basic equations for a magnetoelectroelastic solid

In the Cartesian coordinate system x_i (i=1,2,3), the governing equations for magnetoelectroelastic materials can be written as [36]:

$$\begin{cases} \sigma_{ij} = c_{ijks}\varepsilon_{ks} - e_{sij}E_s - h_{sij}H_s, \\ D_i = e_{iks}\varepsilon_{ks} + \alpha_{is}E_s + d_{is}H_s, \\ B_i = h_{iks}\varepsilon_{ks} + d_{is}E_s + \mu_{is}H_s, \end{cases} \tag{1}$$

$$\varepsilon_{ij} = \frac{1}{2}\left(u_{i,j} + u_{j,i}\right), \quad E_i = -\varphi_{,i}, \quad H_i = -\phi_{,i}, \tag{2}$$

$$\sigma_{ij,j} = 0, \quad D_{i,i} = 0, \quad B_{i,i} = 0, \tag{3}$$

where σ_{ij}, D_i, B_i are the components of the stresses, electrical displacements and magnetic inductions; ε_{ij}, E_i, H_i are the components of strains, electrical and magnetic fields; u_i, φ, ϕ are the mechanical displacement components, electrical and magnetic potentials; c_{ijks}, e_{iks}, h_{iks}, d_{is} are the elastic, piezoelectric, piezomagnetic, and electromagnetic constants; α_{is}, μ_{si} are the dielectric permittivity and magnetic permeability coefficients; Indices i, j, k, s range from 1 to 3, with repeated ones implying summation, and the comma stands for the differentiation with respect to the coordinate variables. We further point out that in writing eqs. (1)–(3), we have assumed that the system is free of any mechanical, electric or magnetic source, and that the deformation is linear.

From eqs. (1)–(3), one gets the following governing equations:

$$\begin{cases} \left(c_{ijks}u_k + e_{sij}\varphi + h_{sij}\phi\right)_{,si} = 0, \\ \left(e_{iks}u_k - \alpha_{is}\varphi - d_{is}\phi\right)_{,si} = 0, \\ \left(h_{iks}u_k - d_{is}\varphi - \mu_{is}\phi\right)_{,si} = 0. \end{cases} \tag{4}$$

We now further assume that all the field quantities are independent of the second coordinate x_2. Then, making use of the Lekhnitskii-Eshelby-Stroh representation and extending it to the magnetoelectroelastic material, a general solution to eq. (4) can be presented in the form [36]:

$$V = Af(z) + \overline{Af}(\overline{z}), \tag{5}$$

$$t = Bf'(z) + \overline{Bf}'(\overline{z}), \tag{6}$$

where the prime $(')$ denotes differentiation with respect to the argument, and an overbar stands for the complex conjugate. Also in eqs. (5) and (6):

$$\boldsymbol{V} = [u_1, \; u_2, \; u_3, \; \varphi, \; \phi]^{\mathrm{T}}, \tag{7}$$

$$\boldsymbol{t} = [\sigma_{31}, \; \sigma_{32}, \; \sigma_{33}, \; D_3, \; B_3]^{\mathrm{T}}, \tag{8}$$

$$\boldsymbol{f}(z) = [f_1(z_1), \; f_2(z_2), \; f_3(z_3), \; f_4(z_4), \; f_5(z_5)]^{\mathrm{T}}, \tag{9}$$

with the superscript ‘T’ standing for the transposed matrix and $z_j = x_1 + p_j x_3 \; (j = 1, 2, \cdots, 5)$. The matrix $\boldsymbol{A}$ has the following expression:

$$\boldsymbol{A} = [\boldsymbol{A}_1, \; \boldsymbol{A}_2, \; \boldsymbol{A}_3, \; \boldsymbol{A}_4, \; \boldsymbol{A}_5]^{\mathrm{T}}, \tag{10}$$

with p_j and $\boldsymbol{A}_j = [a_{1j}, \; a_{2j}, \; a_{3j}, \; a_{4j}, \; a_{5j}]^{\mathrm{T}}$ being, respectively, the eigenvalue and eigenvector of the system:

$$\left[\boldsymbol{Q} + p_j(\boldsymbol{R} + \boldsymbol{R}^{\mathrm{T}}) + p_j^2 \boldsymbol{T}\right]\boldsymbol{A}_j = 0. \tag{11}$$

In eq. (11), the elements of the 5×5 matrices $\boldsymbol{Q}$, $\boldsymbol{R}$ and $\boldsymbol{T}$ are defined as:

$$\boldsymbol{Q} = \begin{bmatrix} \boldsymbol{Q}^{\mathrm{E}} & \boldsymbol{e}_{11} & \boldsymbol{h}_{11} \\ \boldsymbol{e}_{11}^{\mathrm{T}} & -\alpha_{11} & -d_{11} \\ \boldsymbol{h}_{11}^{\mathrm{T}} & -d_{11} & -\mu_{11} \end{bmatrix},$$

$$\boldsymbol{R} = \begin{bmatrix} \boldsymbol{R}^{\mathrm{E}} & \boldsymbol{e}_{31} & \boldsymbol{h}_{31} \\ \boldsymbol{e}_{13}^{\mathrm{T}} & -\alpha_{13} & -d_{13} \\ \boldsymbol{h}_{13}^{\mathrm{T}} & -d_{13} & -\mu_{13} \end{bmatrix}, \tag{12}$$

$$\boldsymbol{T} = \begin{bmatrix} \boldsymbol{R}^{\mathrm{E}} & \boldsymbol{e}_{33} & \boldsymbol{h}_{33} \\ \boldsymbol{e}_{33}^{\mathrm{T}} & -\alpha_{33} & -d_{33} \\ \boldsymbol{h}_{33}^{\mathrm{T}} & -d_{33} & -\mu_{33} \end{bmatrix}$$

and

$$\begin{aligned} &(\boldsymbol{Q}^{\mathrm{E}})_{jk} = c_{1jk1}, \; (\boldsymbol{R}^{\mathrm{E}})_{jk} = c_{1jk3}, \\ &(\boldsymbol{T}^{\mathrm{E}})_{jk} = c_{3jk3}, \; (\boldsymbol{e}_{ij})_m = e_{ijm}, (\boldsymbol{h}_{ij})_m = h_{ijm}. \end{aligned} \tag{13}$$

The 5×5 matrix $\boldsymbol{B}$ can be found by

$$\boldsymbol{B} = (\boldsymbol{R}^{\mathrm{T}} + \boldsymbol{PT})\boldsymbol{A} \tag{14}$$

with $\boldsymbol{P} = \mathrm{diag}[p_1, \; p_2, \; p_3, \; p_4, \; p_5]$.

We consider the transversely isotropic magnetoelectroelastic material which is poled in the x_3-direction. Then, the displacement V_3 of the vector-function $\boldsymbol{V}$ decouples, in the (x_1, x_3)-plane, from the components $(V_1, \; V_3, \; V_4, \; V_5)$. Thus, in the following sections, our attention will be focused on this generalized plane strain problem for the components $(V_1, \; V_3, \; V_4, \; V_5)$.

3 Statement of the problem and solutions

3.1 A magnetoelectroelastic bimaterial plane with an interface crack

A bimaterial composed of two dissimilar magnetoelectroelastic semi-infinite planes $x_3 > 0$ and $x_3 < 0$ with material properties defined, respectively, by the following material constants $c_{ijks}^{(1)}$, $e_{iks}^{(1)}$, $h_{iks}^{(1)}$, $d_{is}^{(1)}$, $\alpha_{is}^{(1)}$, $\mu_{si}^{(1)}$ and $c_{ijks}^{(2)}$, $e_{iks}^{(2)}$, $h_{iks}^{(2)}$, $d_{is}^{(2)}$, $\alpha_{is}^{(2)}$, $\mu_{si}^{(2)}$, is considered (Figure 1, with superscripts “(1)” and “(2)” denoting, respectively, the field quantities in materials 1 and 2). We assume that the extended vector $\boldsymbol{t}$ is continuous across the whole bimaterial interface, that the part $L = (-\infty, c) \cup (b, \infty)$ of the interface $-\infty < x_1 < \infty, x_3 = 0$ is magnetoelectromechanically bounded, and that the crack surfaces are extended traction-free for $x_1 \in [c, a] = L_1$ whilst they should be in frictionless contact for $x_1 \in (a, b) = L_2$, and the position of the point a is arbitrarily chosen for the time being. Furthermore, we assume that a pair of oppositely directed concentrated forces $\boldsymbol{X} = -[\tau_0, \; \sigma_0, \; d_0, \; b_0]^{\mathrm{T}} \delta(x_1 - d)$ are applied at $x_1 = d$ on the crack faces, where $\tau_0, \sigma_0, d_0, b_0$ are, respectively, the applied uniform normal stress, uniform shear stress, uniform electrical displacement and uniform magnetic induction. In addition, we assume that the influence of one

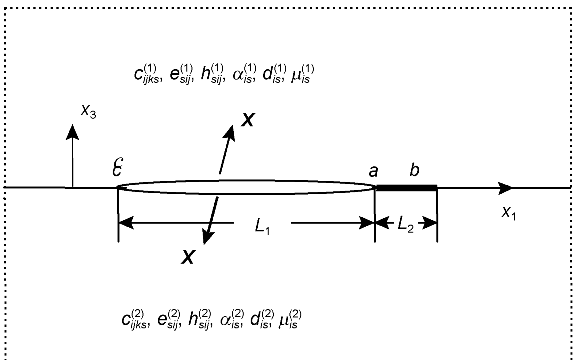

Figure 1 An interface crack with a contact zone between two dissimilar semi-infinite magnetoelectroelastic planes under concentrated magneto-electromechanical loads.

contact zone upon the other is negligibly small [46,51], and thus, in the present study only the contact zone at the right crack tip is considered. Certainly, a contact zone at the left crack-tip can be treated similarly [50].

For the present interface crack problem, the continuity and boundary conditions at the interface can be written in the following form:

$$\left[\boldsymbol{V}\left(x_1\right)\right]=\mathbf{0},\ \left[\boldsymbol{t}\left(x_1\right)\right]=\mathbf{0},\ x_1\in L, \tag{15a}$$

$$\begin{aligned}&\left[\sigma_{31}^{(m)},\quad \sigma_{33}^{(m)},\quad B_3^{(m)}\right]^{\mathrm{T}}\\&\quad=-\left[\tau_0,\quad \sigma_0,\quad b_0\right]^{\mathrm{T}}\delta\left(x_1-d\right),\\&\left[\varphi\left(x_1\right)\right]=0,\left[D_3\left(x_1\right)\right]=0,\ x_1\in L_1,\end{aligned} \tag{15b}$$

$$\begin{cases}\sigma_{31}^{(m)}\left(x_1,0\right)=0,\ \left[\sigma_{33}\left(x_1\right)\right]=0,\\ \left[D_3\left(x_1\right)\right]=0,\ \left[B_3\left(x_1\right)\right]=0,\\ \left[u_3\left(x_1\right)\right]=0,\ \left[\varphi\left(x_1\right)\right]=0,\left[\phi\left(x_1\right)\right]=0,\end{cases}\quad x_1\in L_2, \tag{15c}$$

where

$$\begin{aligned}&\left[\Upsilon\left(x_1\right)\right]=\Upsilon^{+}\left(x_1,0\right)-\Upsilon^{-}\left(x_1,0\right),\\&\Upsilon=\boldsymbol{V},\boldsymbol{t},u_3,\varphi,\phi,\sigma_{33},D_3,B_3.\end{aligned} \tag{16}$$

In eq. (16), the signs "+" and "–" denote the value on the upper and lower face of the interface.

It should be pointed out that the electrical displacement on the crack surfaces $x_1\in L_1$ consists of two parts. The first is the imposed $-d_0\delta\left(x_1-d\right)$, and the second is the unknown caused by

$$-\left[\tau_0,\quad \sigma_0,\quad b_0\right]^{\mathrm{T}}\delta\left(x_1-d\right).$$

3.2 The magnetoelectroelastic solution

Similar to eq. [50], from eqs. (5), (6) and (15), the following expressions at the interface are obtained

$$\begin{aligned}\left[\boldsymbol{V}'\left(x_1\right)\right]&=\left[V_1'(x_1),\quad V_3'(x_1),\quad V_4'(x_1),\quad V_5'(x_1)\right]^{\mathrm{T}}\\&=\boldsymbol{W}^{+}\left(x_1\right)-\boldsymbol{W}^{-}\left(x_1\right),\end{aligned} \tag{17}$$

$$\begin{aligned}\boldsymbol{t}^{(1)}\left(x_1,0\right)&=\left[\sigma_{31}^{(1)},\quad \sigma_{33}^{(1)},\quad D_3^{(1)},\quad B_3^{(1)}\right]^{\mathrm{T}}\\&=\boldsymbol{G}\boldsymbol{W}^{+}\left(x_1\right)-\bar{\boldsymbol{G}}\boldsymbol{W}^{-}\left(x_1\right),\end{aligned} \tag{18}$$

where $\boldsymbol{W}(z)=\left[W_1(z),\quad W_3(z),\quad W_4(z),\quad W_5(z)\right]^{\mathrm{T}}$ is an introduced unknown vector function, and $\boldsymbol{W}^{+}(x_1)=\boldsymbol{W}\left(x_1+\mathrm{i}0\right)$, $\boldsymbol{W}^{-}\left(x_1\right)=\boldsymbol{W}\left(x_1-\mathrm{i}0\right)$; the matrix $\boldsymbol{G}$ is related to the following known matrix $\tilde{\boldsymbol{G}}$ defined by

$$\tilde{\boldsymbol{G}}=\boldsymbol{B}^{(1)}\boldsymbol{D}^{-1} \tag{19}$$

with

$$\boldsymbol{D}=\boldsymbol{A}^{(1)}-\bar{\boldsymbol{L}}\boldsymbol{B}^{(1)} \tag{20}$$

and

$$\boldsymbol{L}=\boldsymbol{A}^{(2)}\left(\boldsymbol{B}^{(2)}\right)^{-1}. \tag{21}$$

It is worth noticing that the matrix $\boldsymbol{G}$ and the vector $\boldsymbol{W}(z)$ are related to the matrix $\ddot{\boldsymbol{H}}$ (or $\ddot{\boldsymbol{N}}$) and the vector function $\ddot{\boldsymbol{\omega}}(z)$ (or $\ddot{\boldsymbol{\Phi}}'(z)$) in [36] (or [37]) by $\mathrm{i}\boldsymbol{G}^{-1}=\ddot{\boldsymbol{H}}\left(=\ddot{\boldsymbol{N}}^{-1}\right)$ and $\boldsymbol{W}(z)=-\mathrm{i}\ddot{\boldsymbol{\omega}}(z)\left(=\ddot{\boldsymbol{\Phi}}'(z)\right)$, respectively, where all the quantities with the overhead sign "$\ddot{\ldots}$" denote the corresponding quantities in refs. [36] and/or [37]. In addition, it should be pointed out that the matrix $\boldsymbol{G}$ has the following structure [50]:

$$\boldsymbol{G}=\begin{bmatrix}G_{11}&G_{12}&G_{13}&G_{14}\\G_{21}&G_{22}&G_{23}&G_{24}\\G_{31}&G_{32}&G_{33}&G_{34}\\G_{41}&G_{42}&G_{43}&G_{44}\end{bmatrix}=\begin{bmatrix}\mathrm{i}\tilde{g}_{11}&\tilde{g}_{13}&\tilde{g}_{14}&\tilde{g}_{15}\\\tilde{g}_{31}&\mathrm{i}\tilde{g}_{33}&\mathrm{i}\tilde{g}_{34}&\mathrm{i}\tilde{g}_{35}\\\tilde{g}_{41}&\mathrm{i}\tilde{g}_{43}&\mathrm{i}\tilde{g}_{44}&\mathrm{i}\tilde{g}_{45}\\\tilde{g}_{51}&\mathrm{i}\tilde{g}_{53}&\mathrm{i}\tilde{g}_{54}&\mathrm{i}\tilde{g}_{55}\end{bmatrix}, \tag{22}$$

where all $\tilde{g}_{ij}$ are real, and $\tilde{g}_{31}=-\tilde{g}_{13}$, $\tilde{g}_{41}=-\tilde{g}_{14}$, $\tilde{g}_{51}=-\tilde{g}_{15}$, $\tilde{g}_{43}=\tilde{g}_{34}$, $\tilde{g}_{53}=\tilde{g}_{35}$, $\tilde{g}_{54}=\tilde{g}_{45}$. And it is easily known from eqs. (17) and (18) that for the considered crack surface conditions, $W_4^{+}\left(x_1\right)=W_4^{-}\left(x_1\right)=0$.

With a row matrix $\boldsymbol{S}=\left[S_1,\quad S_3,\quad S_5\right]$ introduced and a product $\boldsymbol{S}\hat{\boldsymbol{t}}^{(1)}\left(x_1,0\right)$ considered with

$$\hat{\boldsymbol{t}}^{(1)}\left(x_1,0\right)=\left[\sigma_{31}^{(1)}\left(x_1,0\right),\quad \sigma_{33}^{(1)}\left(x_1,0\right),\quad B_3^{(1)}\left(x_1,0\right)\right]^{\mathrm{T}},$$

the following relations can be obtained by using eqs. (17) and (18):

$$\begin{aligned}&\sigma_{33}^{(1)}\left(x_1,0\right)+m_{j5}B_3^{(1)}\left(x_1,0\right)+\mathrm{i}m_{j1}\sigma_{13}^{(1)}\left(x_1,0\right)\\&\quad=\Omega_j^{+}\left(x_1\right)+\gamma_j\Omega_j^{-}\left(x_1\right),\end{aligned} \tag{23}$$

$$\begin{aligned}&n_{j1}\left[u_1'\left(x_1\right)\right]+\mathrm{i}n_{j3}\left[u_3'\left(x_1\right)\right]+\mathrm{i}n_{j5}\left[\phi'\left(x_1\right)\right]\\&\quad=\Omega_j^{+}\left(x_1\right)-\Omega_j^{-}\left(x_1\right),\end{aligned} \tag{24}$$

where

$$\Omega_j\left(z\right)=n_{j1}W_1\left(z\right)+\mathrm{i}\left(n_{j3}W_3\left(z\right)+n_{j5}W_5\left(z\right)\right) \tag{25}$$

and $m_{j5}=S_{j5}$, $m_{j1}=-\mathrm{i}S_{j1}$, $n_{j1}=Y_{j1}$, $n_{j3}=-\mathrm{i}Y_{j3}$, $n_{j5}=$

$-\mathrm{i}Y_{j5}$, $\boldsymbol{Y}_j=\boldsymbol{S}_j\hat{\boldsymbol{G}}$. γ_j and $\boldsymbol{S}_j^{\mathrm{T}}=\left[S_{j1},\ S_{j3},\ S_{j5}\right]^{\mathrm{T}}$ $(j=1,3,5)$ are, respectively, the eigenvalues and eigenvectors of the matrix $\left(\gamma\hat{\boldsymbol{G}}^{\mathrm{T}}+\bar{\tilde{\boldsymbol{G}}}^{\mathrm{T}}\right)$ with

$$\hat{\boldsymbol{G}}=\begin{bmatrix}\mathrm{i}\tilde{g}_{11} & \tilde{g}_{13} & \tilde{g}_{15}\\ \tilde{g}_{31} & \mathrm{i}\tilde{g}_{33} & \mathrm{i}\tilde{g}_{35}\\ \tilde{g}_{51} & \mathrm{i}\tilde{g}_{53} & \mathrm{i}\tilde{g}_{55}\end{bmatrix}.$$

In addition, as shown in ref. [50], here m_{jl}, n_{jl} $(j,l=1,3,5)$ are all real.

Using eqs. (23) and (24) for $j=1,5$, and the corresponding interface conditions and boundary conditions at infinity, one can derive the following combined Dirichlet-Riemann boundary value problem:

$$\Omega_j^+(x_1)+\gamma_j\Omega_j^-(x_1)=-\left(\sigma_0+m_{j5}b_0+im_{j1}\tau_0\right)\delta(x_1-d),\quad x_1\in L_1, \tag{26}$$

$$\operatorname{Im}\Omega_j^{\pm}(x_1)=0,\quad x_1\in L_2, \tag{27}$$

$$\Omega_j(z)\big|_{z\to\infty}=0, \tag{28}$$

where “Im” stands for the imaginary part of the complex quantity.

The exact analytical solutions to eqs. (26) and (27) for $j=1,5$ under the conditions at infinity (28) can be expressed as follows:

$$\Omega_j(z)=\frac{X_j(z)}{d-z}\left[\operatorname{Re}\left(I_{0j}\right)+\mathrm{i}\operatorname{Im}\left(I_{0j}\right)\frac{Y(z)}{Y(d)}\right], \tag{29}$$

where “Re” stands for the real part of the complex quantity, and

$$X_j(z)=\mathrm{e}^{\mathrm{i}\varpi_j(z)}\Big/\sqrt{(z-c)(z-a)},$$
$$I_{0j}=-\frac{1}{2\pi\mathrm{i}}\frac{\sigma_0+m_{j5}b_0+\mathrm{i}m_{j1}\tau_0}{X_j^+(d)}, \tag{30}$$
$$Y(z)=\sqrt{(z-a)/(z-b)}$$

with

$$\varpi_j(z)=2\varepsilon_j\ln\frac{\sqrt{(b-a)(z-c)}}{\sqrt{l(z-a)}+\sqrt{(a-c)(z-b)}},$$
$$\varepsilon_j=\frac{1}{2\pi}\ln\gamma_j,\quad l=b-c. \tag{31}$$

Using eqs. (29), (23) and (24) for $j=1$, one can get the following expressions at the interface, for $x_1>b$ (ahead of the contact zone):

$$\sigma_{33}^{(1)}(x_1,0)+m_{15}B_3^{(1)}(x_1,0)+\mathrm{i}m_{11}\sigma_{13}^{(1)}(x_1,0)=\left[\frac{\operatorname{Re}(I_{01})}{\sqrt{(x_1-a)}}+\mathrm{i}\operatorname{Im}(I_{01})\frac{\sqrt{(b-d)/(a-d)}}{\sqrt{(x_1-b)}}\right]\times\frac{(1+\gamma_1)\exp\left[\mathrm{i}\varpi_1(x_1)\right]}{(d-x_1)\sqrt{(x_1-c)}}, \tag{32}$$

for $x_1\in L_2$ (within the contact zone):

$$\begin{aligned}\sigma_{33}^{(1)}(x_1,0)+m_{15}B_3^{(1)}(x_1,0)&=\frac{(1+\gamma_1)\operatorname{Re}(I_{01})}{(d-x_1)\sqrt{(x_1-c)(x_1-a)}}\times\left[\cosh\varpi_0(x_1)+\frac{1-\gamma_1}{1+\gamma_1}\sinh\varpi_0(x_1)\right]\\&-\frac{(1+\gamma_1)\sqrt{(b-d)/(a-d)}\operatorname{Im}(I_{01})}{(d-x_1)\sqrt{(x_1-c)(b-x_1)}}\times\left[\sinh\varpi_0(x_1)+\frac{1-\gamma_1}{1+\gamma_1}\cos\varpi_0(x_1)\right],\end{aligned} \tag{33a}$$

$$\left[u_1'(x_1)\right]=\frac{2}{n_{11}\sqrt{x_1-c}}\left[\frac{\operatorname{Re}(I_{01})\sinh\varpi_0(x_1)}{(d-x_1)\sqrt{(x_1-a)}}-\frac{\operatorname{Im}(I_{01})\sqrt{(b-d)/(a-d)}\cos\varpi_0(x_1)}{(d-x_1)\sqrt{(b-x_1)}}\right], \tag{33b}$$

for $x_1\in L_1$ (in the open part of the crack):

$$n_{11}\left[u_1'(x_1)\right]+\mathrm{i}\left\{n_{13}\left[u_3'(x_1)\right]+n_{15}\left[\phi'(x_1)\right]\right\}=2\sqrt{\alpha_1}\left[\frac{\sqrt{(b-d)/(a-d)}\operatorname{Im}(I_{01})}{(d-x_1)\sqrt{b-x_1}}-\mathrm{i}\frac{\operatorname{Re}(I_{01})}{(d-x_1)\sqrt{a-x_1}}\right]\times\frac{\exp\left[\mathrm{i}\varpi^*(x_1)\right]}{\sqrt{x_1-c}}, \tag{34}$$

where

$$\varpi_0(x_1)=2\varepsilon_1\tan^{-1}\sqrt{\frac{(a-c)(b-x_1)}{(b-c)(x_1-a)}},$$
$$\varpi^*(x_1)=2\varepsilon_1\ln\frac{\sqrt{(b-a)(x_1-c)}}{\sqrt{l(a-x_1)}+\sqrt{(a-c)(b-x_1)}}, \tag{35}$$

$\alpha_1=\dfrac{(1+\gamma_1)^2}{4\gamma_1}$, and $\operatorname{Re}(I_{01}),\operatorname{Im}(I_{01})$ can be simplified as:

$$\mathrm{Re}(I_{01}) = -\frac{l\sqrt{(1-\theta)(\theta-\lambda)}}{2\pi\sqrt{\gamma_1}}\omega_1, \quad \mathrm{Im}(I_{01}) = \frac{l\sqrt{(1-\theta)(\theta-\lambda)}}{2\pi\sqrt{\gamma_1}}\omega_2 \tag{36}$$

with

$$\omega_1 = \Sigma_1 \cos\kappa(\lambda) + m_{11}\tau_0 \sin\kappa(\lambda), \quad \omega_2 = \left[\Sigma_1 \sin\kappa(\lambda) - m_{11}\tau_0 \cos\kappa(\lambda)\right], \tag{37a}$$

$$\Sigma_1 = \sigma_0 + m_{15}b_0, \quad \kappa(\lambda) = 2\varepsilon_1 \ln\frac{\sqrt{\lambda(1-\theta)}}{\sqrt{\theta-\lambda}+\sqrt{\theta(1-\lambda)}}, \tag{37b}$$

$$\theta = \frac{b-d}{b-c}, \ \lambda = \frac{b-a}{b-c}.$$

For the magnetically impermeable and electrically permeable interface crack, eqs. (32)–(34) are not sufficient for obtaining all necessary characteristics at the interface. Therefore, eqs. (23) and (24) for j=5 should be considered. Since m_{51} and n_{51} are all equal to zero, the following expressions at the interface can be further obtained:

$$\sigma_{33}^{(1)}(x_1,0) + m_{55}B_3^{(1)}(x_1,0) = \frac{2\,\mathrm{Re}(I_{05})}{(d-x_1)\sqrt{(x_1-c)(x_1-a)}}, \ x_1 \in L_2, \tag{38}$$

$$n_{53}\left[u_3'(x_1)\right] + n_{55}\left[\phi'(x_1)\right] = -2\frac{\mathrm{Re}(I_{05})}{(d-x_1)\sqrt{(x_1-c)(a-x_1)}}, \ x_1 \in L_1, \tag{39}$$

where $\mathrm{Re}(I_{01}), \mathrm{Im}(I_{01})$ can be expressed as:

$$\mathrm{Re}(I_{05}) = -\frac{\Sigma_5 l\sqrt{(1-\theta)(\theta-\lambda)}}{2\pi\sqrt{\gamma_1}}, \quad \mathrm{Im}(I_{05}) = -m_{11}\tau_0\frac{l\sqrt{(1-\theta)(\theta-\lambda)}}{2\pi\sqrt{\gamma_1}} \tag{40}$$

with $\Sigma_5 = \sigma_0 + m_{55}b_0$.

The stress $\sigma_{33}^{(1)}$ and magnetic induction $B_3^{(1)}$ at $z = x_1 + \mathrm{i}0$ can be easily determined from eqs. (32) and (38) for $x_1 > b$ and from eqs. (33a) and (38) for $x_1 \in L_2$.

Introducing the following field intensity factors (FIFs):

$$K_1 = \lim_{x_1\to a+0}\sqrt{2\pi(x_1-a)}\sigma_{33}(x_1,0), \quad K_2 = \lim_{x_1\to b+0}\sqrt{2\pi(x_1-b)}\sigma_{13}(x_1,0), \tag{41a}$$

$$K_5 = \lim_{x_1\to a+0}\sqrt{2\pi(x_1-a)}B_3(x_1,0), \tag{41b}$$

and using the expressions obtained above, one can finally get

$$K_1 = (m_{55}-m_{15})^{-1}\sqrt{\frac{2(1-\theta)}{\pi l\gamma_1(1-\lambda)(\theta-\lambda)}} \times\left(\sqrt{\gamma_1}m_{55}\omega_1 - m_{55}\Sigma_5\right), \tag{42a}$$

$$K_2 = -\sqrt{\frac{1-\theta}{2\pi l\theta\gamma_1}}\frac{(1+\gamma_1)\omega_2}{m_{11}}, \tag{42b}$$

$$K_5 = -(m_{55}-m_{15})^{-1}\sqrt{\frac{2(1-\theta)}{\pi l\gamma_1(1-\lambda)(\theta-\lambda)}} \times\left(\sqrt{\gamma_1}\omega_1 - \Sigma_5\right). \tag{42c}$$

Making use of eqs. (34) and (39) gives the expressions for $[u_3']$ and $[\phi']$, which for $x_1 \to a-0$ have the following form:

$$[u_3'] = -\frac{1}{\sqrt{2\pi(a-x_1)}}(\Theta_{11}K_1 + \Theta_{15}K_5), \tag{43a}$$

$$[\phi'] = -\frac{1}{\sqrt{2\pi(a-x_1)}}(\Theta_{51}K_1 + \Theta_{55}K_5), \tag{43b}$$

where

$$\Theta_{11} = \left(n_{55}\sqrt{\alpha_1/\gamma_1} - n_{15}\right)\Big/\Delta_n,$$
$$\Theta_{15} = \left(m_{15}n_{55}\sqrt{\alpha_1/\gamma_1} - m_{15}n_{15}\right)\Big/\Delta_n,$$
$$\Theta_{51} = \left(n_{13} - n_{53}\sqrt{\alpha_1/\gamma_1}\right)\Big/\Delta_n,$$
$$\Theta_{55} = \left(m_{55}n_{13} - m_{15}n_{53}\sqrt{\alpha_1/\gamma_1}\right)\Big/\Delta_n,$$
$$\Delta_n = n_{13}n_{55} - n_{53}n_{15}.$$

Moreover, eq. (33b) for $x_1 \to b-0$ leads to

$$[u_1'] = -\frac{1}{\sqrt{2\pi(b-x_1)}}\Theta_2 K_2, \tag{44}$$

where

$$\Theta_{22} = -\frac{2m_{11}}{n_{11}(1+\gamma_1)}. \tag{45}$$

Further, we introduce the energy release rates (ERRs) related to the points a and b:

$$G_1 = \lim_{\Delta l\to 0}\frac{1}{2\Delta l}\int_a^{a+\Delta l}\left\{\sigma_{33}^{(1)}(x_1,0)\left[u_3(x_1-\Delta l,0)\right]\right.$$

$$+B_3^{(1)}(x_1,0)\left[\phi(x_1-\Delta l,0)\right]\}\mathrm{d}x_1, \tag{46}$$

$$G_2=\lim_{\Delta l\to 0}\frac{1}{2\Delta l}\int_b^{b+\Delta l}\sigma_{31}^{(1)}(x_1,0)\left[u_1(x_1-\Delta l,0)\right]\mathrm{d}x_1. \tag{47}$$

Integrating eqs. (43) and (44), and substituting the results, along with the corresponding expressions for $\sigma_{33}^{(1)}(x_1,0)$, $B_3^{(1)}(x_1,0)$ and $\sigma_{31}^{(1)}(x_1,0)$ obtained previously, into eqs. (46) and (47), one gets the following expressions:

$$G_1=\frac{\Theta_{11}K_1^2+\Theta_{55}K_5^2+(\Theta_{15}+\Theta_{51})K_1K_5}{4}, \tag{48}$$

$$G_2=\frac{\Theta_{22}K_2^2}{4}. \tag{49}$$

The total ERR G is the sum of G_1 and G_2.

With $\left[u_2'(x_1)\right]=W_1^+(x_1)-W_1^-(x_1)$ being considered, the three components in eq. (18) can be written in the form:

$$\begin{bmatrix}\sigma_{33}^{(1)}(x_1,0)\\ D_3^{(1)}(x_1,0)\\ B_3^{(1)}(x_1,0)\end{bmatrix}=\begin{bmatrix}\tilde g_{31}\\ \tilde g_{41}\\ \tilde g_{51}\end{bmatrix}\left[u_1'(x_1)\right]+\mathrm{i}\begin{bmatrix}\tilde g_{33} & \tilde g_{34} & \tilde g_{35}\\ \tilde g_{43} & \tilde g_{44} & \tilde g_{45}\\ \tilde g_{53} & \tilde g_{54} & \tilde g_{55}\end{bmatrix}\times\begin{bmatrix}W_3^+(x_1)+W_3^-(x_1)\\ 0\\ W_5^+(x_1)+W_5^-(x_1)\end{bmatrix}. \tag{50}$$

The first and third equations of eq. (50) can be solved for $W_3^+(x_1)+W_3^-(x_1)$ and $W_5^+(x_1)+W_5^-(x_1)$. Then substituting the results back into the second equation of eq. (50) leads to the expression of $D_3^{(1)}(x_1,0)$ in terms of $\sigma_{33}^{(1)}(x_1,0)$, $B_3^{(1)}(x_1,0)$ and $\left[u_1'(x_1)\right]$. Thus, the following expression for electrical displacement intensity factor at $x_1=a+0$ can be finally derived:

$$K_4=\lim_{x_1\to a+0}\sqrt{2\pi(x_1-a)}D_3(x_1,0)=\theta_1K_1+\theta_5K_5, \tag{51}$$

where

$$\theta_1=(\tilde g_{41}+p_3)\gamma_0+p_1,\ \theta_5=(\tilde g_{41}+p_3)\gamma_0m_{15}+p_2 \tag{52}$$

with

$$\begin{aligned}&\gamma_0=(\gamma_1-1)/(n_{11}\gamma_1),\\ &p_1=(\tilde g_{43}\tilde g_{55}-\tilde g_{45}\tilde g_{53})/\Delta_0,\\ &p_2=(\tilde g_{45}\tilde g_{33}-\tilde g_{43}\tilde g_{35})/\Delta_0,\end{aligned} \tag{53}$$

$$\begin{aligned}&p_3=(\tilde g_{43}\tilde g_{35}\tilde g_{51}+\tilde g_{45}\tilde g_{53}\tilde g_{31}-\tilde g_{43}\tilde g_{55}\tilde g_{31}-\tilde g_{45}\tilde g_{33}\tilde g_{51})/\Delta_0,\\ &\Delta_0=\tilde g_{55}\tilde g_{33}-\tilde g_{53}\tilde g_{35}.\end{aligned} \tag{54}$$

It is worth mentioning that all the normal stress, electrical displacement and magnetic induction are also singular in the left crack tip $x_1=b-0$. By introducing the following FIFs:

$$\begin{bmatrix}K_1^b\\ K_4^b\\ K_5^b\end{bmatrix}=\lim_{x_1\to b-0}\sqrt{2\pi(b-x_1)}\begin{bmatrix}\sigma_{33}(x_1,0)\\ D_3(x_1,0)\\ B_3(x_1,0)\end{bmatrix} \tag{55}$$

and using $\sigma_{33}^{(1)}(x_1,0)$, $B_3^{(1)}(x_1,0)$ obtained from eqs. (33) and (38) and with consideration of eq. (50), one can get

$$\begin{aligned}&K_1^b=\frac{m_{11}m_{55}(1-\gamma_1)}{(m_{15}-m_{55})(1+\gamma_1)}K_2,\ K_4^b=-\frac{K_1^b}{m_{55}},\\ &K_5^b=-(\tilde g_{41}+p_3)\frac{2m_{11}}{n_{11}(1+\gamma_1)}K_2+p_1K_1^b+p_2K_4^b.\end{aligned} \tag{56}$$

Eq. (56) implies that all FIFs K_1^b, K_4^b and K_5^b are completely defined by the shear SIF K_2 at $x_1=b+0$. In addition, it can be easily proved that all the normal stress, electrical displacement and magnetic induction in the right crack-tip $x_1=b+0$ are nonsingular, which is in agreement with the interface crack problem for purely elastic bimaterials [43,53].

By following the same procedure, solutions to other crack surface conditions can be derived similarly. These solutions, along with the physical meanings of different crack surface conditions are given in Appendix A.

3.3 Determination of the contact zone

The solution to the interface crack problem obtained in the previous section is mathematically correct for any crack tip location $x_1=a$. However, it only becomes physically valid if the following inequalities are satisfied:

$$\begin{cases}\sigma_{33}^{(1)}(x_1,0)\leqslant 0, & x_1\in L_2,\\ \left[u_3\right]\geqslant 0, & x_1\in L_1.\end{cases} \tag{57}$$

An analytical analysis and numerical verifications show that these inequalities hold true only if a is taken from the segment $[a_1,a_2]$ providing $a_1\leqslant a_2$, where

$$a_1=b-\lambda_1 l,\ a_2=b-\lambda_2 l, \tag{58}$$

λ_1 is the maximum root in the interval $(0,1)$ of the equation (K_1 in eq. (42a)):

$$K_1=0 \tag{59}$$

and λ_2 is the similar root of the equation ($\left[u_3'\right]$ in eq. (43a)):

$$\sqrt{a-x_1}\left[u_3'\left(x_1,0\right)\right]=0. \tag{60}$$

Therefore, eqs. (59) and (60), connecting to eqs. (42a) and (43a), can be solved numerically for λ_1 and λ_2.

In addition, usually the real contact zone length $\lambda_0=\dfrac{b-a}{l}$ is uniquely defined by inequalities (57), and then the contact zone model in the Comninou [43] sense will take place. For the case considered, a set of positions $a\in\left[a_1,a_2\right]$ providing $\left(a_1\leqslant a_2\right)$ satisfy the inequalities (58). In other words this set can be defined as follows:

$$\Omega_a=\left[a\geqslant a_1\cap a\leqslant a_2\right]. \tag{61}$$

Obviously, if $\Omega_a=\varnothing$, the contact zone model considered here does not exist. Thus, the most interesting situation is associated with $\Omega_a\neq\varnothing$ and it is clear that for any of such cases a unique contact zone defined by a real position of the point a should exist.

4 Numerical results and discussions

In this section, some typical numerical calculations are carried out. In all our numerical procedures, σ_0 and τ_0 are, respectively, normalized by σ_0/σ and τ_0/σ, where without loss of generality, $\sigma=4.2\times10^6\ \mathrm{N/m^2}$; and $\lambda_B=b_0\,h_{33}^{(1)}\big/\left(\sigma\mu_{33}^{(1)}\right)$ is the loading combination parameter introduced to reflect the corresponding loading combination between magnetic and mechanical loads. In addition, in our numerical examples, the interface crack between two dissimilar $CoFe_2O_4$-$BaTiO_3$ composites is considered. Their material properties as volume percentage (or volume fraction) v_f of $BaTiO_3$ were given by Sih and Song [54] in detail. In what follows, material 1 and material 2 correspond to $CoFe_2O_4$-$BaTiO_3$ composites with $v_f=0.1$ and $v_f=0.9$, respectively. For convenience, their material constants are listed in Table 1 [54,50]. The crack length l=2 mm is assumed. Numerical results are plotted in Figures 2–10, where $K_0=\sigma\big/\sqrt{0.5l}$ and $G_0=K_0^2/4$.

Figures 2–4 show the effects of the location of the applied concentrated loads on the contact zone length λ_0, the normalized Mode-II SIFs K_2/K_0 and the normalized total energy release rate G/G_0 for different shear loads with fixed σ_0/σ=1 and λ_B=0, respectively. It is observed clearly from these figures that with increasing θ (i.e., decreasing d), the contact zone length increases, and both the Mode-II SIF and energy release rate decrease. Furthermore, Figures 3 and 4

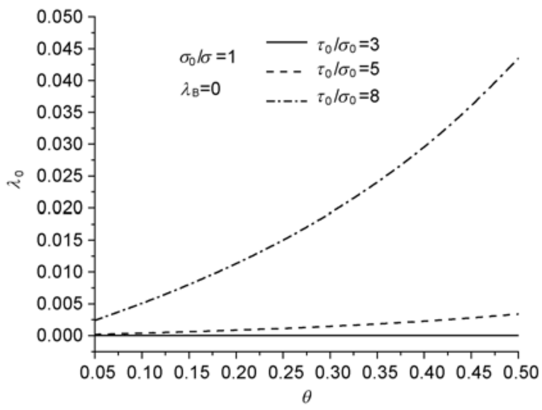

Figure 2 Contact zone length λ_0 (=$(b-a)/l$) versus the location of the applied concentrated loads θ(=$(b-d)/(b-c)$) for different shear loads as σ_0/σ=1 and λ_B=0 (Equivalent to b_0=0).

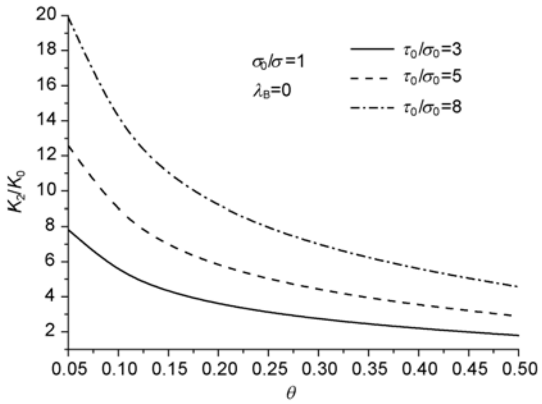

Figure 3 Normalized Mode-II SIFs K_2/K_0 (at $x_1=b+0$) versus the position of the applied concentrated loads for different shear loads as σ_0/σ=1 and λ_B=0.

Table 1 Material constants for $BaTiO_3$-$CoFe_2O_4$ composites with different volume fractions (v_f) [50,54]

Material constants	v_f=0.1	v_f=0.9	Material constants	v_f=0.1	v_f=0.9
c_{11} (GPa)	274	178.0	$\alpha_{11}\times10^{-10}$ (C^2/N m^2)	11.9	100.9
c_{13} (GPa)	161	87.2	$\alpha_{33}\times10^{-10}$ (C^2/N m^2)	13.4	113.5
c_{33} (GPa)	259	172.8	h_{32} (N/A m)	522.3	58.03
c_{44} (GPa)	45	43.2	h_{33} (N/A m)	629.7	69.97
e_{31} (C/m^2)	–4.4	–3.96	h_{15} (N/A m)	495.0	55.00
e_{33} (C/m^2)	1.86	16.74	$\gamma_{11}\times10^{-6}$ (N s^2/C^2)	531.5	63.5
e_{15} (C/m^2)	1.16	10.44	$\gamma_{33}\times10^{-6}$ (N s^2/C^2)	142.3	24.7

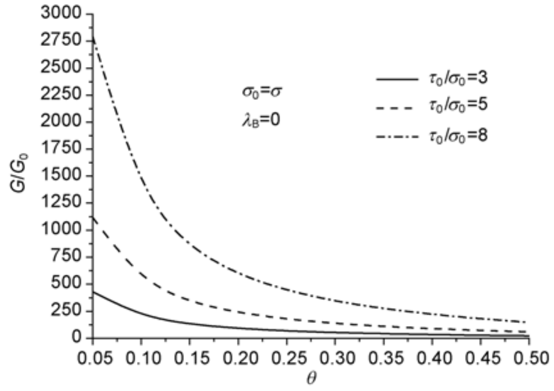

Figure 4 Normalized total energy release rates versus the position of the applied concentrated loads for different shear loads as σ_0/σ=1 and λ_B=0.

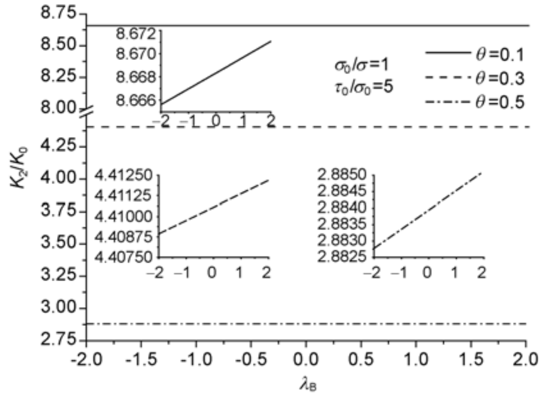

Figure 6 Normalized Mode-II SIFs K_2/K_0 (at x_1=b+0) versus the applied magnetic load λ_B for different positions of the applied concentrated loads as σ_0/σ=1 and τ_0/σ_0=5.

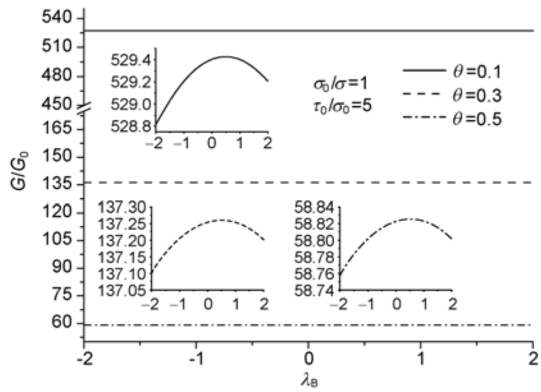

Figure 7 Normalized total energy release rates versus the applied magnetic load λ_B for different positions of the applied concentrated loads as σ_0/σ=1 and τ_0/σ_0=5.

imply that for the present load cases, the total energy release rate and Mode-II SIF can both be used equivalently as fracture parameter. Thus, according to the maximum energy release rate criterion, the nearer to the left crack-tip the applied concentrated combined mechanical loads approach, the easier growth and propagation the crack right tip is. We point out that for the electrically impermeable and magnetically permeable case and the electromagnetically permeable case, similar behaviors (but with slightly different amplitudes) can be obtained with Figures 2 and 3 being further close to those in ref. [50] for the electromagnetically permeable case.

Figures 5–7 show the effects of the magnetical load λ_B on the contact zone length λ_0, the normalized Mode-II SIF K_2/K_0 and the normalized total energy release rate G/G_0 for different locations of the concentrated loads with fixed σ_0/σ=1 and τ_0/σ_0=5, respectively. Figures 5–7 indicate that with increasing λ_B, the contact zone length generally decreases whilst the Mode-II SIFs increase. It is also interesting that the directions of the magnetic load could slightly affect the energy release rates. On the other hand, it should be noted that the effects of magnetic loads on any one of the contact zone length, Mode-II SIF and energy release rate are insignificant. This feature holds also for the electrically impermeable and magnetically permeable case.

Figures 8–10 display the effects of the normalized applied shear load on the contact zone length λ_0, the normalized Mode-II SIFs K_2/K_0 and the normalized total energy release rate G/G_0 for different magnetic loads with fixed

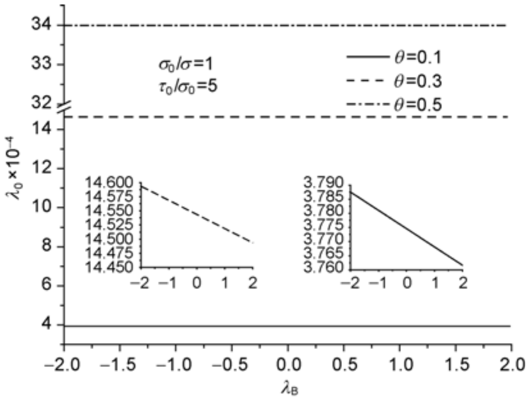

Figure 5 Contact zone lengths versus the applied magnetic load λ_B for different positions of the applied concentrated loads as σ_0/σ=1 and τ_0/σ_0=5.

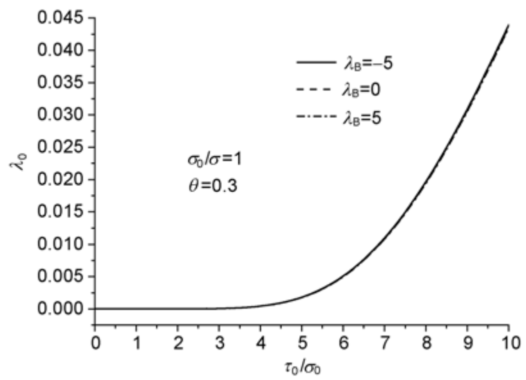

Figure 8 Contact zone lengths versus the normalized applied shear load for different magnetic loads as σ_0/σ=1 and θ=0.3.

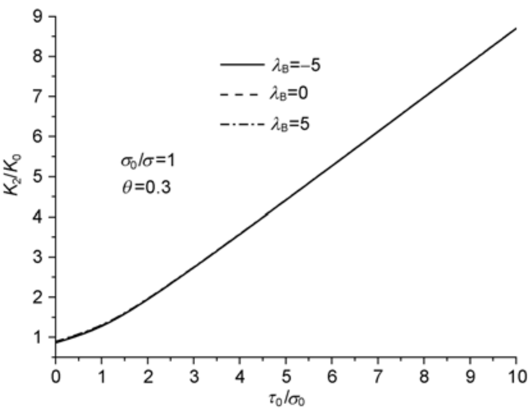

Figure 9 Normalized Mode-II SIFs K_2/K_0 (at $x_1=b+0$) versus the normalized applied shear load for different magnetic loads as $\sigma_0/\sigma=1$ and $\theta=0.3$.

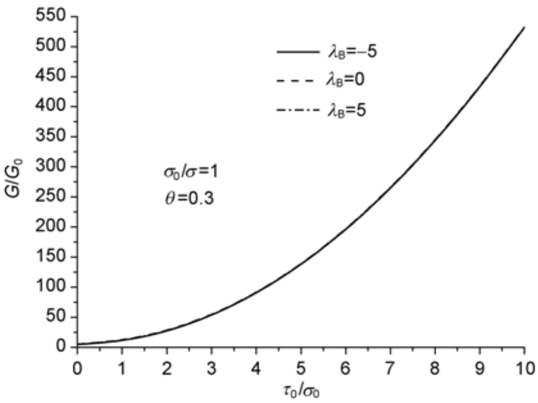

Figure 10 Normalized total energy release rates versus the normalized applied shear load for different magnetic loads as $\sigma_0/\sigma=1$ and $\theta=0.3$.

$\sigma_0/\sigma=1$ and $\theta=0.3$, respectively. As shown in these figures, for a fixed position of the applied concentrated loads, in general, λ_0, K_2 and G all increase with the increase of applied shear load. Figures 8–10 also imply that magnetic loads have negligible effects on λ_0, K_2 and G. Figure 10 further indicates that according to the energy release rate criterion, the crack easily initiates and grows with increasing shear load.

For the electromagnetically permeable case, Figures 11–13 show, respectively, the variation of the contact zone length λ_0, the normalized Mode-II SIF K_2/K_0, and the normalized total energy release rate G/G_0 vs. the normalized applied shear load, for different θ with fixed $\sigma_0/\sigma=1$. It is shown clearly that the contact zone length increases with increasing applied load and with increasing θ (or decreasing d). Both the Mode-II SIF and total energy release rate also increase with increasing applied load but with decreasing θ (or increasing d).

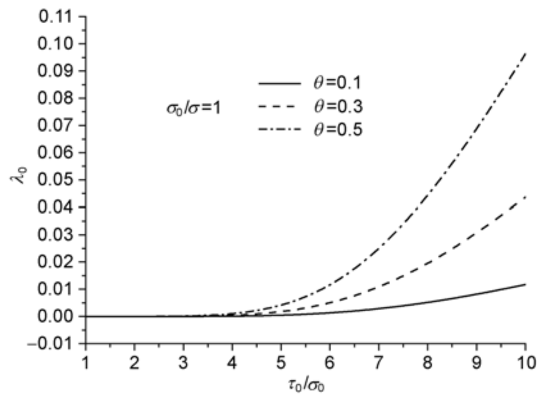

Figure 11 Contact zone length versus the normalized applied shear load for the electromagnetically permeable case with fixed $\sigma_0/\sigma=1$ but different θ.

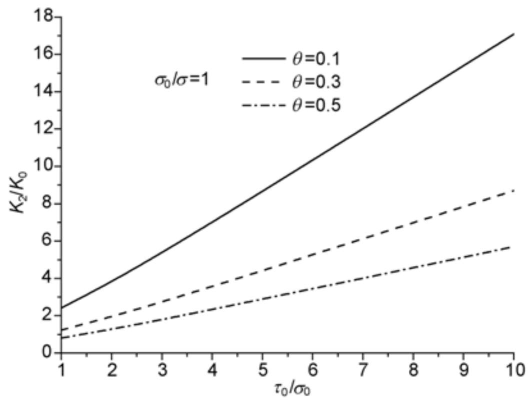

Figure 12 Normalized Mode-II SIFs K_2/K_0 (at $x_1=b+0$) versus the normalized applied shear load for the electromagnetically permeable case with fixed $\sigma_0/\sigma=1$ but different θ.

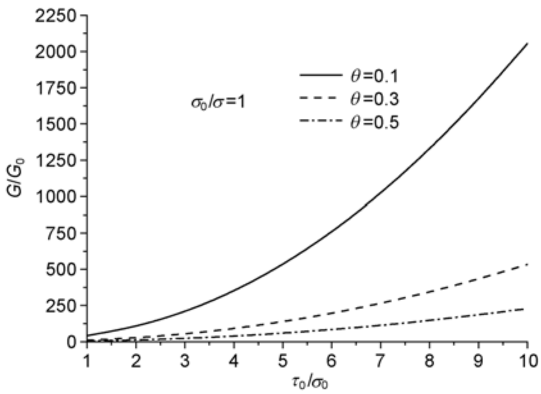

Figure 13 Normalized total energy release rates versus the normalized applied shear load for the electromagnetically permeable case with fixed $\sigma_0/\sigma=1$ but different θ.

5 Conclusions

An interface crack with a contact zone in an infinite magnetoelectroelastic bimaterial under the concentrated magnetoelectromechanical loads at the crack faces has been considered. For the open part of the crack faces, magnetically impermeable and electrically permeable crack surface condition is adopted. First, the matrix-vector representations (17) and (18) for the stresses, electrical displacement and magnetic induction as well as for the derivatives of the jumps of the displacements, electrical and magnetic potentials via a sectionally-holomorphic vector-function are given. Next, the combined Dirichlet-Riemann boundary value problems (26)–(28) are derived and solved. Then, the stress, electrical displacement and magnetic induction intensity factors as well as the energy release rate have been obtained in a concise and analytical form. The transcendental equations for the determination of real contact zone length have been obtained as well. Finally, some typical numerical results are given for the material combination of $BaTiO_3$-$CoFe_2O_4$ composites. From the theoretical and numerical results, the following conclusions can be drawn:

(1) For the magnetically impermeable and electrically permeable interface crack with a contact zone under concentrated magnetoelectromechanical loads, all the normal stress, electrical displacement and magnetic induction at the right crack-tip a exhibit a square-root singularity, and the electrical displacement intensity factor at $x_1=a+0$ depends on the Mode-I stress and magnetic induction intensity factors at $x_1=a+0$.

(2) Although all the normal stress, electrical displacement and magnetic induction at the right crack-tip $x_1=b+0$ are nonsingular, all of them are singular at the left crack tip $x_1=b-0$. Furthermore, all the field intensity factors K_1^b, K_4^b and K_5^b at the left crack-tip $x_1=b-0$ are completely defined by the shear SIF K_2 at $x_1=b+0$, which reflects the intensity of square-root singularity of the shear stress there.

(3) For the crack model with contact zone, the Mode-II SIF plays a very important role in the fracture analysis of the interface crack because it is nearly equivalent to total energy release rate.

(4) For a fixed size of the applied magnetoelectromechanical load, the contact zone length generally increases with decreasing load location parameter d. For a fixed location of the concentrated loads, the contact zone length increases with increasing shear load.

(5) According to the maximum energy release rate criterion, in general, the nearer to the left crack-tip $x_1=c$ the concentrated combined mechanical loads, the easier to grow and propagate the crack right-tip $x_1=b$ is. Moreover, the crack easily initiates and grows with increasing applied shear load.

(6) For the present crack model, in general, the magnetic loads have a negligible effect on the contact zone length, Mode-II SIF and energy release rate.

(7) Solutions to the other interface crack conditions are also presented and the corresponding numerical results are further discussed to illustrate the possible effect of different electromagnetic conditions on the field quantities.

Appendix A Solutions to interface crack conditions

There exist various interface crack surface conditions which are very useful in practical engineering analysis. For example, for the one we discussed mostly in this paper, the magnetically impermeable condition is actually magnetically open whilst the electrically permeable is electrically closed (i.e., it is an electrical wall). This and other electromagnetic conditions are quite common in electromagnetic studies [55–58]. As such, we add below the results for other two common crack surface electromagnetic conditions for easy future reference.

A1 The electrically impermeable and magnetically permeable interface crack

Following the same procedure, we find that

$$K_1=\left(m_{44}-m_{14}\right)^{-1}\sqrt{\frac{2(1-\theta)}{\pi l\gamma_1(1-\lambda)(\theta-\lambda)}}\times\left(\sqrt{\gamma_1}m_{44}\omega_1-m_{14}\Sigma_4\right),\tag{a1}$$

$$K_2=-\sqrt{\frac{1-\theta}{2\pi l\theta\gamma_1}}\frac{(1+\gamma_1)\omega_2}{m_{11}},\tag{a2}$$

$$K_4=-\left(m_{44}-m_{14}\right)^{-1}\sqrt{\frac{2(1-\theta)}{\pi l\gamma_1(1-\lambda)(\theta-\lambda)}}\times\left(\sqrt{\gamma_1}\omega_1-\Sigma_4\right),\tag{a3}$$

where

$$\omega_1=\Sigma_1\cos\kappa(\lambda)+m_{11}\tau_0\sin\kappa(\lambda),$$

$$\omega_2=\left[\Sigma_1\sin\kappa(\lambda)-m_{11}\tau_0\cos\kappa(\lambda)\right],$$

$$\Sigma_1=\sigma_0+m_{14}d_0,\quad \Sigma_4=\sigma_0+m_{44}d_0.$$

Also, similar to the electrically permeable and magnetically impermeable case, we have $m_{j4}=S_{j4}$, $m_{j1}=-\mathrm{i}S_{j1}$, $n_{j1}=Y_{j1}$, $n_{j3}=-\mathrm{i}Y_{j3}$, $n_{j4}=-\mathrm{i}Y_{j4}$, $\boldsymbol{Y}_j=\boldsymbol{S}_j\hat{\boldsymbol{G}}$, with γ_j and $\boldsymbol{S}_j^{\mathrm{T}}=\left[S_{j1},\ S_{j3},\ S_{j4}\right]^{\mathrm{T}}$ $(j=1,3,4)$ being, respectively, the eigenvalues and eigenvectors of the matrix $\left(\gamma\hat{\boldsymbol{G}}^{\mathrm{T}}+\bar{\hat{\boldsymbol{G}}}^{\mathrm{T}}\right)$ where

$$\hat{\boldsymbol{G}}=\begin{bmatrix}\mathrm{i}\tilde{g}_{11} & \tilde{g}_{13} & \tilde{g}_{14}\\ \tilde{g}_{31} & \mathrm{i}\tilde{g}_{33} & \mathrm{i}\tilde{g}_{34}\\ \tilde{g}_{41} & \mathrm{i}\tilde{g}_{43} & \mathrm{i}\tilde{g}_{44}\end{bmatrix}.$$

Again, as shown in ref. [50], m_{jl}, n_{jl} $(j,l=1,3,4)$ are all real values.

The energy release rate for the case can be expressed as:

$$G_1 = \frac{\Theta_{11} K_1^2 + \Theta_{44} K_4^2 + (\Theta_{14} + \Theta_{41}) K_1 K_4}{4}, \tag{a4}$$

$$G_2 = \frac{\Theta_{22} K_2^2}{4}, \tag{a5}$$

where

$$\Theta_{11} = \left(n_{44}\sqrt{\alpha_1/\gamma_1} - n_{14}\right)\Big/\Delta_n,$$

$$\Theta_{22} = -\frac{2m_{11}}{n_{11}(1+\gamma_1)},$$

$$\Theta_{14} = \left(m_{14} n_{44}\sqrt{\alpha_1/\gamma_1} - m_{14} n_{14}\right)\Big/\Delta_n,$$

$$\Theta_{41} = \left(n_{13} - n_{43}\sqrt{\alpha_1/\gamma_1}\right)\Big/\Delta_n,$$

$$\Theta_{44} = \left(m_{44} n_{13} - m_{14} n_{43}\sqrt{\alpha_1/\gamma_1}\right)\Big/\Delta_n,$$

$$\Delta_n = n_{13} n_{44} - n_{43} n_{14}.$$

In addition, the magnetic induction intensity factor at $x_1=a+0$ can be finally derived as follows:

$$K_5 = \theta_1 K_1 + \theta_4 K_4, \tag{a6}$$

where

$$\theta_1 = (\tilde{g}_{51} + p_3)\gamma_0 + p_1,\ \theta_4 = (\tilde{g}_{51} + p_3)\gamma_0 m_{14} + p_2$$

with

$$\gamma_0 = (\gamma_1 - 1)/(n_{11}\gamma_1),$$
$$p_1 = (\tilde{g}_{53}\tilde{g}_{44} - \tilde{g}_{54}\tilde{g}_{43})/\Delta_0,\ p_2 = (\tilde{g}_{54}\tilde{g}_{33} - \tilde{g}_{53}\tilde{g}_{34})/\Delta_0,$$
$$p_3 = (\tilde{g}_{53}\tilde{g}_{34}\tilde{g}_{41} + \tilde{g}_{54}\tilde{g}_{43}\tilde{g}_{31} - \tilde{g}_{53}\tilde{g}_{44}\tilde{g}_{31} - \tilde{g}_{54}\tilde{g}_{33}\tilde{g}_{41})/\Delta_0,$$
$$\Delta_0 = \tilde{g}_{44}\tilde{g}_{33} - \tilde{g}_{43}\tilde{g}_{34}.$$

Furthermore, all the FIFs K_1^b, K_4^b and K_5^b are completely defined by the shear SIF K_2 at $x_1 = b+0$. In other words

$$K_1^b = \frac{m_{11} m_{44}(1-\gamma_1)}{(m_{14} - m_{44})(1+\gamma_1)} K_2,$$

$$K_5^b = -\frac{K_1^b}{m_{44}}, \tag{a7}$$

$$K_4^b = -(\tilde{g}_{51} + p_3)\frac{2m_{11}}{n_{11}(1+\gamma_1)} K_2 + p_1 K_1^b + p_2 K_5^b.$$

A2 The electrically permeable and magnetically permeable interface crack

For this case, we find that

$$K_1 = \sqrt{\frac{2(1-\theta)}{\pi l(1-\lambda)(\theta-\lambda)}}$$
$$\times\left[\sigma_0 \cos\kappa(\lambda) + m_1 \tau_0 \sin\kappa(\lambda)\right], \tag{a8}$$

$$K_2 = -\sqrt{\frac{1-\theta}{2\pi l\theta\gamma_1}}\frac{(1+\gamma_1)}{m_1}\sqrt{(m_1\tau_0)^2 + \sigma_0{}^2}, \tag{a9}$$

where

$$m_1 = -\sqrt{-\frac{\tilde{g}_{31}\tilde{g}_{33}}{\tilde{g}_{11}\tilde{g}_{13}}}.$$

The energy release rate can be written as:

$$G_1 = \frac{\Theta_{11} K_1^2}{4},\quad G_2 = \frac{\Theta_{22} K_2^2}{4}, \tag{a10}$$

where

$$\Theta_{11} = -\frac{\sqrt{\alpha}}{s_1\sqrt{\gamma_1}},\quad \Theta_{22} = -\frac{2m_1}{t_1(1+\gamma_1)},$$

$$t_1 = \tilde{g}_{31} - m_1\tilde{g}_{11},\quad s_1 = (\tilde{g}_{33} + m_1\tilde{g}_{13})/t_1.$$

The electric displacement intensity factor and the magnetic induction intensity factor at $x_1=a+0$ can be finally derived as follows:

$$K_4 = \left[\frac{\tilde{g}_{43}}{\tilde{g}_{33}} + \frac{1-\gamma_1}{2\gamma_1 t_1}\left(\tilde{g}_{41} - \frac{\tilde{g}_{43}\tilde{g}_{31}}{\tilde{g}_{33}}\right)\right] K_1, \tag{a11}$$

$$K_5 = \left[\frac{\tilde{g}_{53}}{\tilde{g}_{33}} + \frac{1-\gamma_1}{2\gamma_1 t_1}\left(\tilde{g}_{51} - \frac{\tilde{g}_{53}\tilde{g}_{31}}{\tilde{g}_{33}}\right)\right] K_1. \tag{a12}$$

Simultaneously, all the FIFs K_1^b, K_4^b and K_5^b are completely defined by the shear SIF K_2 at $x_1 = b+0$, i.e.

$$K_1^b = \frac{m_1(\gamma_1 - 1)}{\gamma_1 + 1} K_2,$$

$$K_4^b = \left(\tilde{g}_{41} - \frac{\tilde{g}_{43}\tilde{g}_{31}}{\tilde{g}_{33}} - \frac{\tilde{g}_{43}}{\tilde{g}_{33}}\right) K_1^b, \tag{a13}$$

$$K_5^b = \left(\tilde{g}_{51} - \frac{\tilde{g}_{53}\tilde{g}_{31}}{\tilde{g}_{33}} - \frac{\tilde{g}_{53}}{\tilde{g}_{33}}\right) K_1^b.$$

This work was supported by the National Natural Science Foundation of China (Grant Nos. 10772123, 11072160), the Program for Changjiang Scholars and Innovative Research Team in University (Grant No. IRT0971) and the Natural Science Fund for Outstanding People of Hebei Province (Grant No. A2009001624).

1 Parton V Z, Kudryavtsev B A. Electromagnetoelasticity. New York:

Gordon and Breach Science Publishers, 1988
2 Zhou Z G, Wang B, Sun Y G. Two collinear interface cracks in magneto-electro-elastic composites. Int J Eng Sci, 2004, 42: 1155–1167
3 Gao C F, Tong P, Zhang T Y. Fracture mechanics for a mode III crack in a magnetoelectroelastic solid. Int J Solids Struct, 2004, 41: 6613–6629
4 Chue C H, Liu T J C. Magneto-electro-elastic antiplane analysis of a bimaterial $BaTiO_3$-$CoFe_2O_4$ composite wedge with an interface crack. Theor Appl Fract Mech, 2005, 44: 275–296
5 Hu K Q, Li G Q. Constant moving crack in a magnetoelectroelastic material under anti-plane shear loading. Int J Solids Struct, 2005, 42: 2823–2835
6 Feng W J, Xue Y, Zou Z Z. Crack growth of an interface crack between two dissimilar magneto-electro-elastic materials under anti-plane mechanical and in-plane electromagnetic impact. Theor Appl Fract Mech, 2005, 43: 376–394
7 Feng W J, Su R K L. Dynamic internal crack problem of a functionally graded magneto-electro-elastic strip. Int J Solids Struct, 2006, 43: 5196–5216
8 Li R, Kardomateas G A. The mode III interface crack in piezo-electro-magneto-elastic dissimilar bimaterials. ASME J Appl Mech, 2006, 73: 220–227
9 Li Y D, Lee K Y. Anti-plane crack intersecting the interface in a bonded smart structure with graded magnetoelectroelastic properties. Theor Appl Fract Mech, 2008, 50: 235–242
10 Zhou Z G, Wang J Z, Wu L Z. The behavior of two parallel non-symmetric interface cracks in a magneto-electro-elastic material strip under an anti-plane shear stress loading. Int J Appl Electromagn Mech, 2009, 29: 163–184
11 Niraula O P, Wang B L. A magneto-electro-elastic material with a penny-shaped crack subjected to temperature loading. Acta Mech, 2006, 187: 151–168
12 Wang B L, Han J C, Mai Y W. Mode III fracture of a magnetoelectroelastic layer: exact solution and discussion of the crack face electromagnetic boundary conditions. Int J Fract, 2006, 139: 27–38
13 Zhao M H, Yang F, Liu T. Analysis of a penny-shaped crack in a magneto-electro-elastic medium. Philos Mag, 2006, 86: 4397–4416
14 Feng WJ, Pan E, Wang X. Dynamic fracture analysis of a penny-shaped crack in a magnetoelectroelastic layer. Int J Solids Struct, 2007, 44: 7955–7974
15 Yong H D, Zhou Y H. Transient response of a cracked manetoelectroelastic strip under anti-plane impact. Int J Solids Struct, 2007, 44: 705-717
16 Wang B L, Sun Y G, Zhang H Y. Analysis of a penny-shaped crack in magnetoelectroelastic materials. J Appl Phys, 2008, 103: 083530-1-8
17 Zhong X C, Zhang K S. Dynamic analysis of a penny-shaped dielectric crack in a magnetoelectroelastic solid under impacts. Eur J Mech A-Solids, 2010, 29: 242–252
18 Li X F. Dynamic analysis of a cracked magnetoelectroelastic medium under antiplane mechanical and inplane electric magnetic impacts. Int J Solids Struct, 2001, 42: 3185–3205
19 Singh B M, Rokne J, Dhaliwal R S. Closed-form solutions for two anti-plane collinear cracks in a magnetoelectroelastic layer. Eur J Mech A-Solids, 2009, 28: 599–609
20 Liu J X, Liu X L, Zhao Y B. Green's functions for anisotropic magnetoelectroelastic solids with an elliptical cavity or a crack. Int J Eng Sci, 2001, 39: 1405–1418
21 Gao C F, Kessler H, Balke H. Crack problems in magnetoelectroelastic solids. Part I: Exact solution of a crack. Int J Eng Sci, 2003, 41: 969–981
22 Gao C F, Kessler H, Balke H. Crack problems in magnetoelectroelastic solids. Part II: General solution of collinear cracks. Int J Eng Sci, 2003, 41: 983–994
23 Song Z F, Sih G C. Crack initiation behavior in magnetoelectroelastic composite under in-plane deformation. Theor Appl Fract Mech, 2003, 39: 189–207
24 Sih G C, Jones R, Song Z F. Piezomagnetic and piezoelectric poling effects on mode I and II crack initiation behavior of magnetoelectroelastic materials. Theor Appl Fract Mech, 2003, 40: 161–186
25 Tian W Y, Gabbert U. Multiple crack interaction problem in magnetoelectroelastic solids. Eur J Mech A-Solids, 2004, 23: 599–614
26 Tian W Y, Gabbert U. Macrocrack-microcrack interaction problem in magnetoelectroelastic solids. Mech Mater, 2005, 37: 565–592
27 Wang B L, Mai YW. Applicability of the crack-face electromagnetic boundary conditions for fracture of magnetoelectroelastic materials. Int J Solids Struct, 2007, 44: 387–398
28 Zhong X C, Li X F. T-stress analysis for a Griffith crack in a magnetoelectroelastic solid. Arch Appl Mech, 2007, 78: 117–125
29 Zhou Z G, Zhang P W, Wu L Z. The closed form solution of a Mode-I crack in the piezoelectric/piezomagnetic materials. Int J Solids Struct, 2007, 44: 419–435
30 Zhou Z G. Wang J Z, Wu L Z. Two collinear Mode-I cracks in piezoelectric/piezomagnetic materials. Struct Eng Mech, 2008, 29: 55–75
31 Chen X H. Energy release rate and path-independent integral in dynamic fracture of magneto-electro-thermo-elastic solids. Int J Solids Struct, 2009, 46: 2706–2711
32 Zhong X C, Liu F, Li X F. Transient response of a magnetoelectroelastic solid with two collinear dielectric cracks under impacts. Int J Solids Struct, 2009, 46: 2950–2958
33 Williams M L. The stresses around a fault or cracks in dissimilar media. Bull Seismol Soc Am, 1959, 49: 199–204
34 Rice J R. Elastic fracture mechanics concept for interfacial cracks. ASME J Appl Mech, 1988, 55: 98–103
35 Gao C F, Tong P, Zhang T Y. Interfacial crack problems in magneto-electric solids. Int J Eng Sci, 2003, 41: 2105–2121
36 Gao C F, Noda N. Thermal-induced interfacial cracking of magnetoelectroelastic material. Int J Eng Sci, 2004, 42: 1347–1360
37 Li R, Kardomateas G A. The mixed mode I and II interface crack in piezoelectromagneto-elastic anisotropic bimaterials. ASME J Appl Mech, 2007, 74: 614–627
38 Feng W J, Su R K L, Liu J X, et al. Fracture analysis of bounded magnetoelectroelastic layers with interfacial cracks under magnetoelectromechanical loads: Plane Problem. J Intell Mater Syst Struct, 2010, 21: 581–594
39 Feng W J, Li Y S, Xu Z H. Transient response of an interfacial crack between dissimilar magnetoelectroelastic layers under magnetoelectromechanical impact loadings: mode-I problem. Int J Solids Struct, 2009, 46: 3346–3356
40 Li X F, Liu G L, Lee K Y. Magnetoelectroelastic field induced by a crack terminating at the interface of a bi-magnetoelectric material. Philos Mag, 2009, 89: 449–463
41 Zhao M H, Li N, Fan CY, et al. Analysis method of planar interface cracks of arbitrary shape in three-dimensional transversely isotropic magnetoelectroelastic bimaterials. Int J Solids Struct, 2008, 45: 1804–1824
42 Zhu B J, Shi Y L, Qin T Y, et al. Mixed-mode stress intensity factors of 3D interface crack in fully coupled electromagnetothermoelastic multiphase composites. Int J Solids Struct, 2010, 46: 2669–2679
43 Comninou M. The interface crack. ASME J Appl Mech, 1977, 44: 631–636
44 Atkinson C. The interface crack with contact zone (an analytical treatment). Int J Fract, 1982, 18: 161–177
45 Simonov I V. The interface crack in homogeneous field of stresses. Mech Compos Mater, 1985, 46: 969–976

46 Dundurs J, Gautesen A K. An opportunistic analysis of the interface crack. Int J Fract, 1988, 36: 151–159

47 Qin Q H, Mai Y W. A closed crack tip model for interface cracks in thermopiezoelectric materials. Int J Solids Struct, 1999, 36: 2463–2479

48 Herrmann K P, Loboda V V. Fracture mechanical assessment of electrically permeable interface cracks in piezoelectric bimaterials by consideration of various contact zone models. Arch Appl Mech, 2000, 70: 127–143

49 Herrmann K P, Loboda V V, Govorukha V B. On contact zone models for an electrically impermeable interface crack in a piezoelectric bimaterial. Int J Fract, 2001, 111: 203–227

50 Herrmann K P, Loboda V V, Khodanen T V. An interface crack with contact zones in a piezoelectric/piezomagnetic bimaterial. Arch Appl Mech, 2010, 80: 651–670

51 Kharun I V, Loboda V V. A set of interface cracks with contact zones in combined tension-shear field. Acta Mech, 2003, 166: 43–56

52 Muskhelishvili N I. Some Basic Problems of the Mathematical Theory of Elasticity. Noordhoff, Leyden, 1975

53 Wang S S, Choi I. The interface crack between two dissimilar anisotropic composite materials. ASME J Appl Mech, 1983, 50: 169–178

54 Sih G C, Song Z F. Magnetic and electric poling effects associated with crack growth in $BaTiO_3$–$CoFe_2O_4$ composite. Theor Appl Fract Mech, 2003, 39: 209–227

55 Papas C H. Theory of Electromagnetic Wave Propagation. New York: Dover, 1988

56 Alshits V I, Barnett D M, Darinskii A N, et al. On the existence problem for localized acoustic waves on the interface between two piezocrystals. Wave Motion, 1994, 20: 233–244

57 Volakis J L, Chatterjee A, Kempel L C. Finite Element Method for Electromagnetics. New York: IEEE Press, 1998

58 Pan E. Some new three-dimensional Green's functions in anisotropic piezoelectric biomaterials. Electron J Bound Elem, 2003, 1: 236–269